J Low Temp Phys (2018) 192:224–240
https://doi.org/10.1007/s10909-018-1952-x

Electron Spin Resonance Studies of Nitrogen Atoms Stabilized in Impurity-Helium Condensates

A. Meraki[1,2] · P. T. McColgan[3] · R. E. Boltnev[4,5] · D. M. Lee[3] · V. V. Khmelenko[3]

Received: 28 February 2018 / Accepted: 2 May 2018 / Published online: 10 May 2018

Abstract Impurity-helium condensates (IHCs) created by injection of nitrogen atoms and molecules as well as rare gas (RG) atoms (Ne, Ar, and Kr) into superfluid ^{4}He have been studied via electron spin resonance (ESR) techniques. We investigated the influence of addition of rare gas atoms (Ne, Ar, and Kr) into the condensing N_2–He gas mixture on the efficiency of stabilization as well as on the local and average concentrations of N atoms attainable in IHCs. Addition of Ar and Kr atoms into the condensing N_2–He gas mixture substantially increased the stabilization efficiency of N atoms in nanoclusters forming IHCs. Measurements of the ground-state spectroscopic parameters of nitrogen atoms show that the nanoclusters have a shell structure. Most of the N atoms reside on solid molecular layers of N_2. These layers form on the surfaces of RG (Ar or Kr) nanoclusters.

Keywords Matrix isolation · Nanoclusters · Electron spin resonance

✉ V. V. Khmelenko
khmel@physics.tamu.edu

1 Department of Physics, Bilecik Seyh Edebali University, 11210 Gulumbe, Bilecik, Turkey

2 TUBITAK-National Metrology Institute, P.O.54, 41470 Gebze, Kocaeli, Turkey

3 Department of Physics and Astronomy and Institute for Quantum Science and Engineering, Texas A&M University, College Station, TX 77843, USA

4 Joint Institue for High Temperatures, Russian Academy of Sciences, Moscow, Russia 125412

5 Branch of Talroze Institute for Energy Problems of Chemical Physics, Russian Academy of Sciences, Chernogolovka, Russia 142432

1 Introduction

The first experimental studies of luminescence from solid nitrogen and solid nitrogen–argon mixtures bombarded by electrons were conducted by Vegard [1,2]. These pioneering studies of solids at low temperature, and in particular rare gases, attracted strong motivation for the investigation of free radicals and ultimately led to development of the matrix isolation method. Later, luminescence of stabilized nitrogen atoms while condensing gas discharge products on a cold substrate was studied by Broida's group [3]. It was expected that slowing down the rate of chemical reactions by lowering temperature could provide large concentrations of stabilized atoms at low temperatures. One goal of these investigations was to create a fuel containing high concentrations of free radicals for rockets and aviation. However, due to the extreme thermal instability of these systems, the accumulation of large enough concentrations of free radicals in solid molecular matrices was not achieved [4].

Impurity-helium condensates (IHCs) are a new class of non-crystalline nanomaterials formed by injecting a beam composed of helium and impurity gases into superfluid helium ^{4}He. Injection of impurity particles after passing through a radio-frequency (RF) discharge zone into superfluid helium allows a considerable increase in the concentration of stabilized atoms in IHCs [5–7]. An RF discharge in the cryostat leads to substantial dissociation of N_2 molecules into N atoms. The pressure gradient inside the cryostat created a well-formed gas jet which was injected into a quartz beaker filled with superfluid helium. IHCs consist of collections of nanoclusters with typical sizes of 3–10 nm, which form a porous gel-like substance inside superfluid helium [8]. Each of the nanoclusters is coated with a few layers of solid helium which impedes the recombination of the stabilized atoms. Ultrasound studies show that IHCs are extremely porous materials with a wide distribution of pore sizes ranging from 8 to 860 nm [9]. The stabilized nitrogen atoms mainly reside on the surfaces of molecular nitrogen nanoclusters [10]. Injection of products of RF discharges into superfluid helium is promising for obtaining high-energy density systems with exceptionally high concentrations of stabilized nitrogen atoms (of order 10^{21} cm^{-3}) in aerogel-like ensembles of nitrogen nanoclusters immersed in superfluid helium. It was found that the addition of Kr atoms to nitrogen–helium, hydrogen–helium, and deuterium–helium gas mixtures used for sample preparation substantially increased the efficiency of N, H, and D atom stabilization [11,12].

There are two main directions for investigating the properties of IHCs. One direction is to examine diffusion processes via recombination of the free radicals in the molecular nanoclusters at low temperatures. Another direction is to study of the structure and dependence of the concentration of stabilized atoms in different matrix environments. Ultrasonic techniques and X-ray diffraction were employed to study the properties of ensembles of nanoclusters [8,13]. Optical spectroscopy was extensively used to investigate the diffusion processes and chemical reactions at low temperatures [14–18]. Electron spin resonance (ESR) techniques were mainly used to investigate the structures of ensembles of nanoclusters and the concentration of stabilized impurity atoms [9,19–21]. In this work, we studied the effects of the addition of rare gas atoms (Ne, Ar, and Kr) into the condensing N_2–He gas mixtures on the efficiency of stabilization of N atoms in IHCs via the ESR technique. We also analyzed the structure

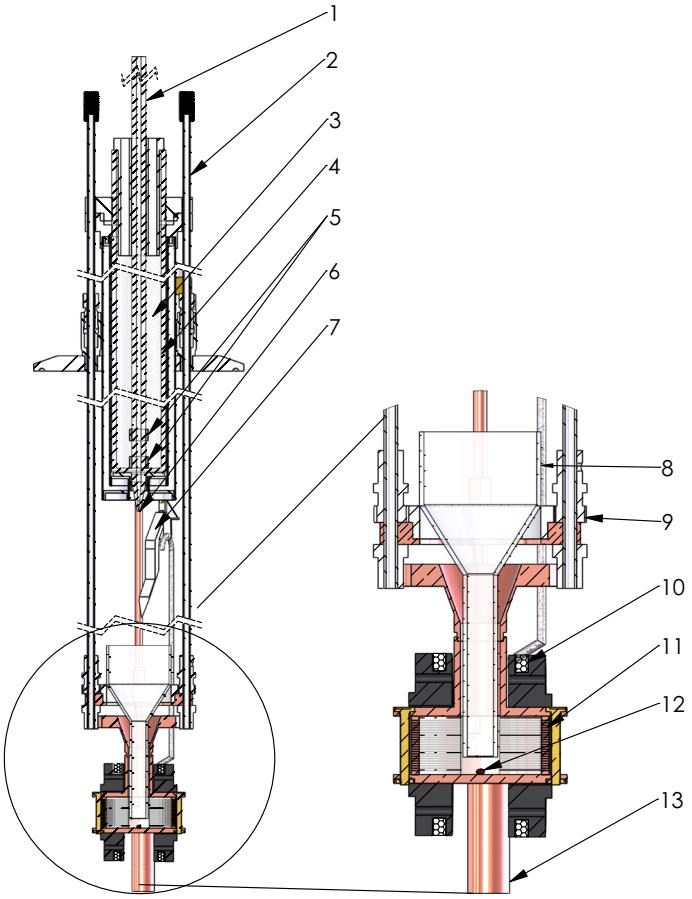

Fig. 1 Low-temperature insert for VTI used in the ESR investigation of IHCs. 1-quartz capillary, 2-tubes for displacement of the beaker in vertical direction, 3-liquid nitrogen, 4-quartz tube, 5-discharge electrodes, 6-orifice, 7-teflon blade, 8-sample collection beaker, 9-beaker rotation gear, 10-modulation coil, 11-horizontal slits on cavity, 12-ruby crystal, 13-fountain pump (Color figure online)

of nanoclusters in samples prepared from the $[N_2]$:[Ne]:[He], $[N_2]$:[Ar]:[He], and $[N_2]$:[Kr]:[He] gas mixtures with this technique.

2 Experimental Method

The experimental setup for simultaneous optical and electron spin resonance (ESR) studies of nanoclusters with stabilized free radicals at low temperatures has been described in more detail elsewhere [22]. The ESR measurements were carried out in a Janis Research liquid helium cryostat with a Bruker spectrometer operating in the X-band ($f \sim 8.91$ GHz). The cryostat tail was centered between the pole faces of a homogeneous Varian 7800 electromagnet. The Janis cryostat contains a variable temperature insert (VTI), which is thermally insulated from the main 4 K helium bath. Most of the ESR measurements were taken for samples immersed in superfluid helium

at ~ 1.33 K which can be achieved by pumping on the VTI with a roots blower backed by a mechanical pump. Figure 1 shows a custom fabricated insert for creation and simultaneous optical and ESR studies of atoms contained in the IHCs. Gas mixtures containing N_2 and neon or argon along with helium gas were prepared in a gas handling system at room temperature and transported through a mass flow controller (a Brooks Model 5850E) with a constant flux of 5×10^{19} particles/s into the cryogenic region. When the prepared gas mixtures pass through a quartz capillary surrounded by liquid nitrogen, a high-power radio-frequency discharge ($f \sim 53$ MHz, power~ 75 W) was applied to electrodes placed around the lower portion of the capillary to dissociate the nitrogen molecules. A gas jet was created as the mixed gases exited through an orifice with diameter 0.75 mm at the bottom of the quartz capillary. The jet impinged on the surface of superfluid helium contained in a small beaker, which was placed 20–25 mm below the orifice. A fountain pump placed at the bottom of the liquid helium bath in the VTI maintained a constant level of superfluid helium in the beaker. The jet is cooled very quickly (the jet temperature drops from 120 to 160 K in the discharge zone down to 2–3 K near the surface of the liquid helium within a few tenths ms) by helium vapor and so the impurity particles (nitrogen molecules, N, O, Ne, and Ar atoms) aggregate into nanoclusters. The oxygen present in the samples is due to a 1ppm contamination in the helium gas. The jet penetrated through the superfluid He surface and a gel-like sample was created. As a result of this process, the sample was accumulated on the conical part of the beaker (see 8 in Fig. 1). A set of teflon blades was employed to scrape the sample from the walls of the funnel while the beaker was rotated so that all of the samples collected onto funnel surface fell into the cylindrical part of the beaker (see Fig. 1). Sample accumulation lasted 10 min. During the sample formation, the temperature 1.5 K was maintained with the aid of the needle valve which supplied liquid helium to the VTI.

Once we have accumulated $\sim 0.3-0.4\,\mathrm{cm}^3$ of sample in the cylindrical part of the beaker, sample accumulation was terminated, and the beaker was lowered from the position near atomic source into the ESR cavity by a pair of stainless steel control tubes. The details of the homemade cylindrical copper cavity can be found elsewhere [22]. The modulation frequency was set at 100 kHz, and derivatives of the ESR absorption lines were obtained at a magnetic field ~ 0.32 T by a lock-in amplifier. Double integration of the ESR spectra gave the number of stabilized N(^{4}S) atoms by comparison with the signal from a ruby crystal (under the same experimental conditions). The ruby crystal was mounted at the bottom of the microwave cavity (see 12 in Fig. 1) and was oriented relative to the main magnetic field in a way such that the ESR lines from the ruby crystal did not overlap with the sample signal. The calibration of the signal from the ruby crystal was made by reference to a diphenyl-picrylhydrazil (DPPH) sample which contained a known number of spins $\sim 2.4\times10^{17}$. ESR measurements provide an estimate for the average and local concentrations of stabilized N(^{4}S) atoms. The average concentrations were determined from the number of stabilized atoms and the volume of 0.35 cm^3 occupied by the samples. The local concentrations were estimated from ESR line broadening due to dipole–dipole interactions. The temperature of the sample was obtained from a germanium thermometer attached to the top of the cavity.

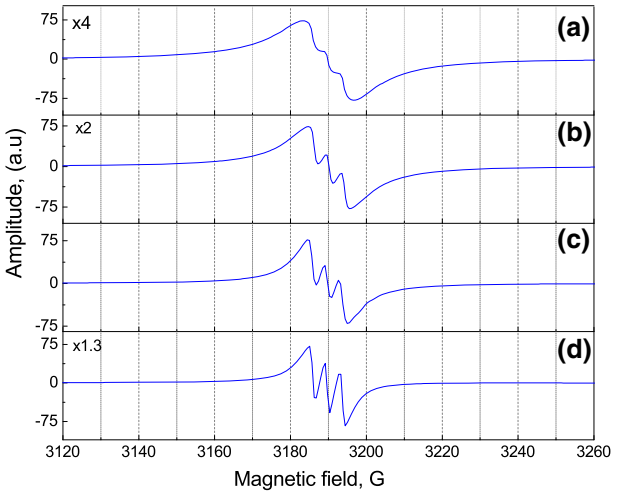

Fig. 2 Experimental ESR spectra of N atoms stabilized in samples prepared from different nitrogen–neon–helium gaseous mixtures: $[N_2]$:[Ne]:[He] = 1:1:50 (a), $[N_2]$:[Ne]:[He] = 1:5:100 (b), $[N_2]$:[Ne]:[He] = 1:20:400 (c), $[N_2]$:[Ne]:[He] = 1:50:1000 (d). All spectra were obtained at 1.33 K (Color figure online)

3 Experimental Results

We performed ESR investigations of the samples formed in HeII by injection of the $[N_2]$:[Ne]:[He] and $[N_2]$:[Ar]:[He] gas mixtures with different ratios. We begin by describing the effect of addition of Ne gas to the nitrogen–helium gas mixtures. The ratio of nitrogen molecules to neon atoms, $[N_2]$/[Ne], in the gas mixtures was varied from 1/50 to 1/1. However, the ratio between impurity gases ($[N_2]$ + [Ne]) and He gas in the mixtures was fixed at the value 1/20. Figure 2 displays the ESR spectra of N atoms in samples prepared from different nitrogen–neon–helium gas mixtures. For the ESR spectra of the sample prepared from gas mixtures with ratios $[N_2]$/[Ne]: 1/1, 1/5, and 1/50, the amplitudes of the signals presented in Fig. 2 were increased by a factor of 4, 2, and 1.3, respectively. We detected very broad ESR spectra of N atoms stabilized in the sample prepared from gas mixture $[N_2]$:[Ne]:[He] = 1:1:50 (see Fig. 2a). The decrease of the $[N_2]$:[Ne] ratio in the condensed gas mixture led to an increase of the amplitude and decrease of broadening of the N atom signal. As we can see in Fig. 2d, the most resolved spectra of N atoms were obtained for the sample prepared from the gas mixture $[N_2]$:[Ne]:[He] = 1:50:1000.

We also studied the effect of adding different quantities of Ar atoms into the nitrogen–helium gas mixtures used for sample preparation on the efficiency of stabilization of N atoms in IHCs. The ratio of nitrogen molecules to argon atoms $[N_2]$/[Ar] in the gas mixture was increased from 1/50 to 1/1. However, the ratio between impurity species ($[N_2]$ + [Ar]) and He in the gas mixture was fixed to the value 1/100. In Fig. 3, one can see that the least resolved ESR spectrum was obtained for the sample prepared from the gas mixture $[N_2]$:[Ar]:[He] = 1:5:600, and the amplitude of the signal was half the size compared to the spectrum obtained from the gas mixture $[N_2]$:[Ar]:[He] = 1:1:200. A more resolved ESR spectrum of N atoms was detected for the sample prepared from the gas mixture $[N_2]$:[Ar]:[He] = 1:20:2000. Further

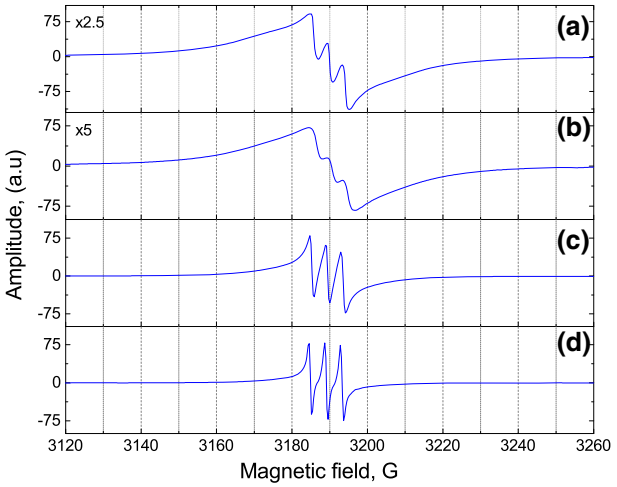

Fig. 3 Experimental ESR spectra of N atoms stabilized in samples prepared from different nitrogen–argon–helium gaseous mixtures: $[N_2]$:[Ar]:[He] = 1:1:200 (a), $[N_2]$:[Ar]:[He] = 1:5:600 (b), $[N_2]$:[Ar]:[He] = 1:20:2000 (c), $[N_2]$:[Ar]:[He] = 1:50:5000 (d). All spectra were obtained at 1.33 K (Color figure online)

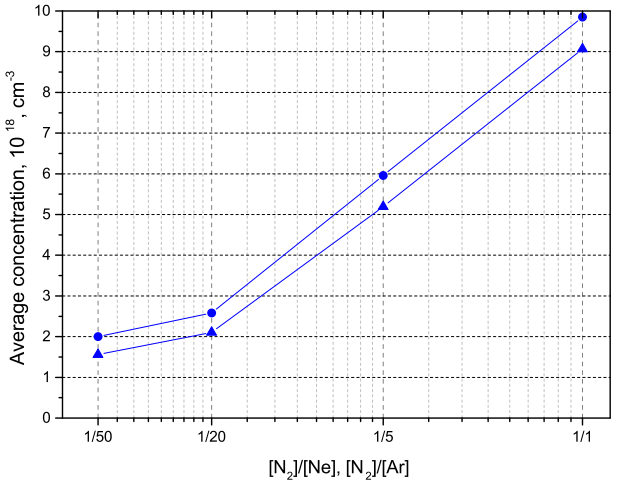

Fig. 4 Dependencies of the average concentration of N atoms stabilized in N_2–Ne–He on N_2/Ne ratio (blue line with triangles) and in N_2–Ar–He samples on the N_2/Ar ratio (blue line with circles) in gas mixtures (Color figure online)

decrease of the $[N_2]$/[Ar] ratio to 1/20 and 1/50 led to even better resolution of the N atom signal. Dependence of the average concentration of N atoms stabilized in N_2–Ne–He and N_2–Ar–He samples on the N_2/Ne and N_2/Ar ratios in gas mixtures used for sample preparation can be seen in Fig. 4. Increasing the concentration of N_2 molecules in nitrogen-rare gas–helium mixtures led to an almost linear growth of N atom concentrations in the samples formed in HeII.

In addition, we investigated two types of samples obtained by condensing nitrogen–helium and nitrogen–krypton–helium gaseous mixtures of different compositions. We

Table 1 Experimental conditions for preparation of IHCs, and average concentrations of N(^{4}S) atoms in IHCs with stabilization efficiency

Gas mixture	Flow rate, $\frac{dN_2}{dt}$, s^{-1}	Average concentration, n_{Ave}, cm^{-3}	N atom stabilization efficiency, κ, %
[$^{14}N_2$]:[He] = 1:100	5.00×10^{17}	5.09×10^{18}	1.0
[$^{14}N_2$]:[He] = 1:400	1.25×10^{17}	2.47×10^{18}	1.95
[$^{14}N_2$]:[He] = 1:800	6.25×10^{16}	1.21×10^{18}	1.90
[$^{14}N_2$]:[Ne]:[He] = 1:1:50	1.00×10^{18}	9.06×10^{18}	0.9
[$^{14}N_2$]:[Ne]:[He] = 1:5:100	5.00×10^{17}	5.19×10^{18}	1.0
[$^{14}N_2$]:[Ne]:[He] = 1:20:400	1.25×10^{17}	2.11×10^{18}	1.7
[$^{14}N_2$]:[Ne]:[He] = 1:50:1000	5.00×10^{16}	1.56×10^{18}	3.1
[$^{14}N_2$]:[Ar]:[He] = 1:1:200	2.50×10^{17}	9.85×10^{18}	4.0
[$^{14}N_2$]:[Ar]:[He] = 1:5:600	8.30×10^{16}	5.96×10^{18}	7.0
[$^{14}N_2$]:[Ar]:[He] = 1:20:2000	2.50×10^{16}	2.58×10^{18}	10.0
[$^{14}N_2$]:[Ar]:[He] = 1:50:5000	1.00×10^{16}	2.00×10^{18}	20.0
[$^{14}N_2$]:[Kr]:[He] = 1:1:400	1.25×10^{17}	9.93×10^{18}	7.7
[$^{14}N_2$]:[Kr]:[He] = 1:2:600	8.33×10^{16}	2.16×10^{19}	25.2
[$^{14}N_2$]:[Kr]:[He] = 1:5:1200	4.16×10^{16}	3.04×10^{19}	70.7

can estimate the average concentration of N atoms in the samples by doubly integrating the derivatives of the ESR signals from the N(^{4}S) atoms and comparing them with the ruby reference signals.

Table 1 gives the conditions of sample preparation and the calculated average concentration of N(^{4}S) atoms as well as the efficiency of stabilization of N atoms in the samples obtained for all of the different gas mixtures. It can be seen from Table 1 that the addition of neon atoms to nitrogen–helium gas mixtures does not substantially affect the efficiency of stabilization of N atoms in the samples. However, the addition of the Ar atoms to nitrogen–helium gas mixtures led to an increase in the efficiency of stabilization of N atoms in nitrogen–argon nanoclusters. The average concentration of N atoms is equal to $\sim 5 \times 10^{18}\,cm^{-3}$ in the sample prepared from the gas mixture [N_2]:[He] = 1:100, whereas for the sample prepared from the gas mixture [N_2]:[Ar]:[He] = 1:1:200, the stabilization efficiency is four times higher than that without the addition of Ar atoms to the N_2–He gas mixture (as shown in Table 1). The average concentration of N atoms in this latter sample is equal to $\sim 1 \times 10^{19}\,cm^{-3}$. It has also been found that addition of Kr atoms to nitrogen–helium gas mixtures leads to an even more significant increase in the average concentration of N atoms in the sample. For instance, for the [N_2]:[He] = 1:400 gas mixture, the average concentration of N(^{4}S) atoms is $\sim 2.5 \times 10^{18}\,cm^{-3}$, whereas for the [$N_2$]:[Kr]:[He] = 1:1:400 gas mixture, it is $\sim 1 \times 10^{19}\,cm^{-3}$. Further addition of Kr atoms to the condensed nitrogen–helium gas mixture led to increasing the stabilization efficiency of N atoms. For gas mixtures [N_2]:[Kr]:[He] = 1:2:600 and [N_2]:[Kr]:[He] = 1:5:1200, the efficiencies of N atom stabilization are 25 and 70%, respectively [23]. The stabilization efficiency (κ) was calculated from the number of nitrogen atoms sent from an RF

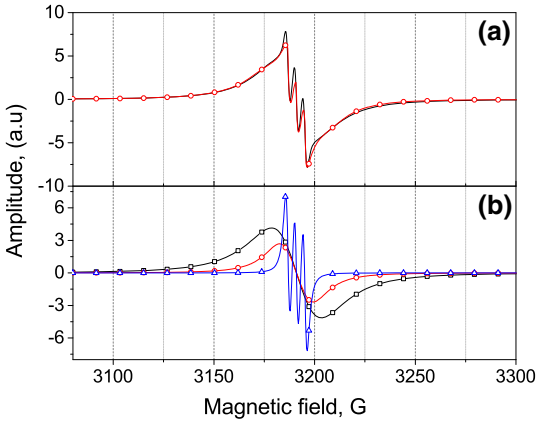

Fig. 5 Experimental ESR spectrum of N atoms for an as-prepared nitrogen–argon–helium sample formed from $[N_2]/[Ar]/[He] = 1/1/200$ gas mixture is shown as a black line (a). The sum of three fitting triplet spectra is shown as red line with circles (a). The three fitting triplet spectra used for decomposing the experimental ESR spectrum are shown in (b): Blue line with triangles is a triplet of Lorentzian lines with the width 2.4 G, red line with circles is a triplet of Lorentzian lines with the width 14.7 G, and black line with squares is a triplet of Lorentzian lines with the width 26.0 G (Color figure online)

discharge into liquid helium from the gas phase jet (N_i) and the number of nitrogen atoms stabilized in sample (N_s) according to the formula:

$$\kappa = \frac{N_s}{N_i} = (n_{Ave} \cdot V_s) / \left(\frac{dN_2}{dt} \cdot t \cdot \sigma \cdot 2 \right), \quad (1)$$

where κ is stabilization efficiency, V_s is the volume of the sample in the beaker which was equal to 0.35 cm^3, $t = 600$ s is the time of accumulation, and σ is the dissociation efficiency of N_2 molecules (of order 30%).

Analysis of the shape and width of the ESR spectra can also provide valuable information about the structure of nanoclusters which form the IHCs and the matrix environments of stabilized nitrogen atoms. For determination of the widths of individual components, and the hyperfine splitting constants, we employed a Mathworks MATLAB Graphic User Interface (GUI) program. The fitting process by the GUI program was described in more detail elsewhere [23]. As seen in Fig. 5a, experimental ESR spectra of the nitrogen atoms in the nitrogen–argon–helium sample can be convoluted as a sum of three triplets of Lorentzian lines. Each of the triplets is assigned to $N(^4S)$ atoms stabilized in different environments. We identify the triplet (red line) in Fig. 5b with N atoms trapped in the Ar matrix ($A = 4.30$ G); the narrow triplet (blue line) in Fig. 5b is assigned to N atoms inside the N_2 nanoclusters ($A = 4.20$ G); and the broad triplet (black line) in Fig. 5b belongs to N atoms residing on the surface of the N_2 nanoclusters ($A = 4.12$ G), where A is the hyperfine constant. ESR linewidths, ΔH_{pp}, local concentrations, n_1, and hyperfine constants, A, of nitrogen atoms in N–Ne–He and N–Ar–He samples obtained from the analysis are shown in Table 2. The spectroscopic characteristics for N atoms in different matrices used for analysis are shown in Table 3. The dipole–dipole electron spin–spin interactions between N atoms

Table 2 Results from analysis of ESR spectra of N atoms for different N_2/Ne/He and N_2/Ar/He samples, where A is the hyperfine structure constant, the g factors are for N atoms, and ΔH_{pp} is the peak to peak width of the fitting ESR spectra

Gas mixture	A, G	ΔH_{pp}	Local concentration, cm^{-3}	Weight, %	g factor
$[^{14}N_2]$:[Ne]:[He] = 1:1:50	4.12	28.47	3.42×10^{20}	69	2.0023
	4.10	10.54	1.26×10^{20}	30.5	2.0018
	4.20	1.34	1.61×10^{19}	0.5	2.0015
$[^{14}N_2]$:[Ne]:[He] = 1:5:100	4.12	23.94	2.87×10^{20}	70.2	2.0025
	4.10	9.23	1.11×10^{20}	28.1	2.0027
	4.20	1.61	1.93×10^{19}	1.6	2.0023
$[^{14}N_2]$:[Ne]:[He] = 1:20:400	4.12	26.58	3.19×10^{20}	69.2	2.0015
	4.10	8.50	1.02×10^{20}	25	2.0022
	4.20	3.20	3.84×10^{19}	5.7	2.0022
$[^{14}N_2]$:[Ne]:[He] = 1:50:1000	4.12	22.17	2.66×10^{20}	73.1	2.0027
	4.10	5.02	6.02×10^{19}	22.6	2.0022
	4.20	1.95	2.34×10^{19}	4.2	2.0026
$[^{14}N_2]$:[Ar]:[He] = 1:1:200	4.12	26.02	3.12×10^{20}	76.5	2.0020
	4.30	14.73	1.77×10^{20}	19.6	2.0023
	4.20	2.40	2.88×10^{19}	3.8	2.0019
$[^{14}N_2]$:[Ar]:[He] = 1:5:600	4.12	27.41	3.29×10^{20}	79.6	2.0028
	4.30	12.37	1.48×10^{20}	18.8	2.0020
	4.20	2.34	2.81×10^{19}	1.5	2.0022
$[^{14}N_2]$:[Ar]:[He] = 1:20:2000	4.12	14.33	1.72×10^{20}	80.1	2.0024
	4.30	6.95	8.34×10^{19}	13.6	2.0018
	4.20	1.19	1.43×10^{19}	6.2	2.0020
$[^{14}N_2]$:[Ar]:[He] = 1:50:5000	4.12	14.06	1.69×10^{20}	70.9	2.0021
	4.30	6.24	7.49×10^{19}	20	2.0017
	4.20	0.76	9.12×10^{18}	9.1	2.0018

lead to broadening of the ESR spectra of the N(^{4}S) atoms. We can determine the local concentration of N atoms in specific environments by having determined the width of an individual triplet for each spectrum. The local concentrations of N(S=3/2) atoms were found from Eq. (2) to be $n_1 = 1.2 \times 10^{19}\Delta H_{pp}$ atoms/cm^3, where ΔH_{pp} is the peak to peak width of the second derivative of ESR absorption signal in Gauss and is related to n_1 and S via the following equation [29]:

$$\Delta H_{pp} = 2.3 g \mu_0 \sqrt{S(S+1)} n_1 \tag{2}$$

We also studied the behavior of the samples during warming through the temperature range of 1.25–20 K. Once the ESR spectra were registered at the temperature $\sim$ 1.33 K, we warmed up the sample to $T \sim 2.16$ K and cooled back down to $T \sim 1.33$ K.

Table 3 Hyperfine structure constants, A, and g factors for N atoms in N_2, Ar, Ne, and Kr matrices and annealed impurity-helium condensates

Matrix	A, G	$(A - A_{free})/A_{free}$ (%)	g factor
Free [24]	3.73	0	2.00215
N_2 [25]	4.22	13.14	2.002155
N_2 [26]	4.21	12.87	2.00201
Ar [27]	4.30	15.28	2.0020
Ne [28]	4.10	9.92	2.0017
Kr [26]	4.47	19.84	2.0012
N_2:Ar:He, Fig. 8c	4.30	15.28	2.00218
N_2:Ne:He, Fig. 8b	4.12	10.46	2.00232
N_2:Ne:He, Fig. 8b'	4.20	12.60	2.00216

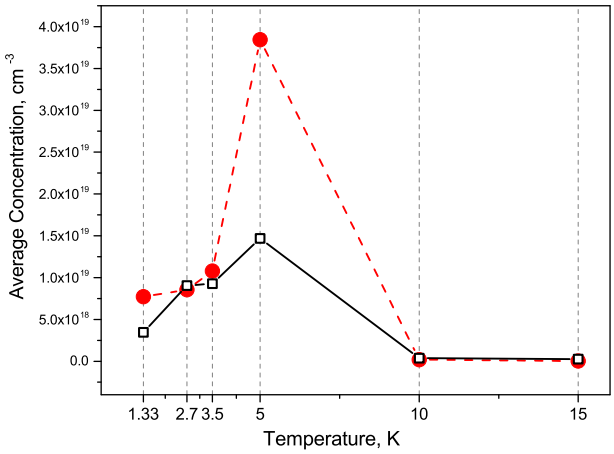

Fig. 6 Dependencies of the average concentration of N atoms on the temperature for samples prepared from $[N_2]/[Ar]/[He] = 1/1/200$ (a red-dash line with circles) and $[N_2]/[Ne]/[He] = 1/1/50$ (a black line with squares) gas mixtures (Color figure online)

At this temperature, again the ESR spectra registrations were performed to see any possible change in the measured ESR signals. This initial warming led to the appearance of thermoluminescence of the sample immersed in HeII and is associated with vortices in the superfluid helium [30]. Figure 6 presents the temperature dependence of the average concentration of N atoms for samples prepared from $[N_2]$:[Ar]:[He] = 1:1:200 and $[N_2]$:[Ne]:[He] = 1:1:50 gas mixtures each showing a maximum at 5 K. The changes of the N atom ESR spectra during annealing of nitrogen–argon–helium samples prepared from $[N_2]$:[Ar]:[He] = 1:1:200 gas mixtures are shown in Fig 7. During heating from 1.3 to 3.5 K, we observed an increase in the intensity of the N atom ESR signals. Further heating to 5 K led to an increasing intensity and width of the N atom ESR signal (see Fig. 7c). Further increasing the sample temperature led to recombination of a majority of the N atoms, leaving only a small well-resolved signal from the remaining atoms (see Fig. 7d). Figure 8 shows experimental spectra of N atoms in the nitrogen–neon–helium and nitrogen–argon–helium samples after annealing to

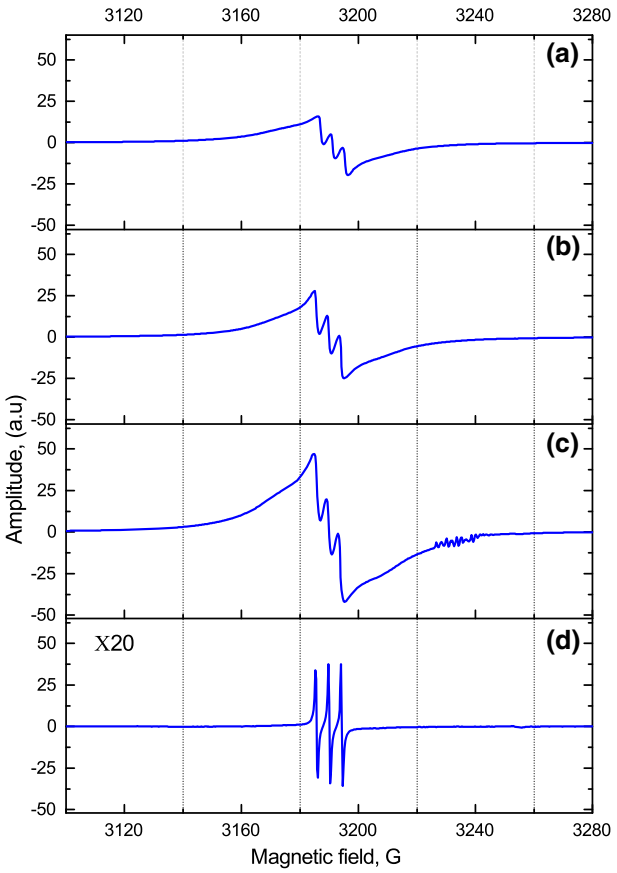

Fig. 7 ESR spectra of nitrogen atoms stabilized in samples prepared with the $[N_2]/[Ar]/[He] = 1/1/200$ gas mixture at $T = 1.3$ K just after accumulation (a), and after sample annealing at different temperatures: 3.5 K (b), 5 K (c), and 10 K (d) (Color figure online)

a temperature of 10 K. The analysis of these spectra is also shown in this figure. The spectrum of N atoms in annealed nitrogen–neon–helium sample was fitted with the sum of two triplet Lorentzian lines as shown in Fig. 8a, b. Even though for the nitrogen–neon–helium sample two triplets of Lorentzian lines were required to adequately fit the data in Fig. 8a, only one triplet of Lorentzian lines (Fig. 8c) is used for fitting the experimental ESR spectrum of N atoms in annealed nitrogen–argon–helium sample.

4 Discussion

Impurity-helium condensates (IHCs) are a new class of non-crystalline nanomaterials formed by injecting a beam composed of helium and impurity gases into superfluid helium. Impurity atoms and/or molecules form nanoclusters in the rapidly cooling gas beam. A shell structure of nanoclusters reflects a stronger interaction of the heavier

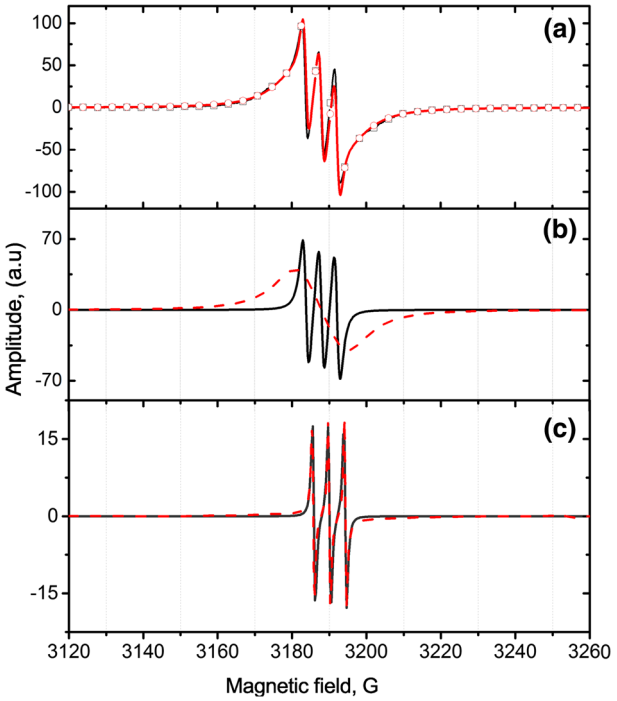

Fig. 8 Analysis of the ESR spectra of N atoms in the samples annealed to 10 K. (a) Experimental ESR spectra of nitrogen atoms stabilized in the nitrogen–neon–helium sample prepared with the $[N_2]/[Ne]/[He] = 1/1/50$ gas mixture, black line with squares. The sum of the fitting lines is shown as red line with circles. (b) The two fitting lines (a red-dash line which is a triplet of Lorentzian lines with the width 16.5 G and $A = 4.12$ G, and a black line which is a triplet of Lorentzian lines with the width 2.8 G and $A = 4.2$ G) are used for decomposing the experimental ESR spectrum. (c) Experimental ESR spectrum of nitrogen atoms stabilized in the nitrogen–argon–helium sample prepared with the $[N_2]/[Ar]/[He] = 1/1/200$ gas mixture is shown as a black line. The triplet of Lorentzian lines with the width 1.2 G and $A = 4.30$ used for fitting the experimental ESR spectrum is shown as red-dash line (Color figure online)

impurities forming nanocluster cores which are surrounded by shells of lighter impurities [23,31]. The impurity nanoclusters are surrounded by one or two layers of solid helium due to the van der Waal forces, which causes them to aggregate into porous, aerogel-like substances inside superfluid helium. We have investigated ensembles of molecular nitrogen nanoclusters bearing high densities of stabilized nitrogen atoms by the ESR technique. The solidified helium shells prevent recombination of atomic free radicals residing on neighboring nanoclusters.

In the present work, we studied the effect of the addition of rare gas atoms (Ne, Ar, and Kr) into the condensing N_2–He gas mixture on the efficiency of stabilization of N atoms in IHCs. In experiments involving krypton–nitrogen–helium jets, particularly high local and average concentrations of N atoms were achieved [23]. The average concentration of nitrogen atoms without addition of RG atoms to N_2–He gas mixture was $\sim 10^{18}$ cm^{-3} and the efficiencies of N atom stabilization for the N_2:He = 1:100 gas mixture were 1%, while for the N_2:He = 1:400 and N_2:He = 1:800 gas mixtures, the efficiencies of N atom stabilization are higher $\sim 2\%$ (see Table 1). Decreasing

Table 4 Parameters of interaction potentials, minimum of energy $\mathcal{E}$ in K (upper numbers), and distance between atoms which corresponds to the potential minimum, R_{min} in Å (lower numbers) of rare gas atoms, oxygen atoms, and nitrogen molecules [32]

Atom/molecule	He	Ne	Ar	Kr	Xe	N_2
He	10.67	18.56	27.84	29.0	29.0	
	2.97	3.2	3.5	3.8	4.1	
Ne	17.4	40.6	68.28	69.6	70.76	
	3.1	3.1	3.5	3.7	3.8	
Ar	25.52	71.92	141.52	150.8	174	
	3.5	3.5	3.76	3.9	4.1	
Kr	25.52	76.56	174	197.2	220.4	
	3.7	3.6	3.8	4.0	4.3	
Xe	25.52	75.4	185.6		266.8	
	4.1	3.8	4.1		4.4	
N_2	27.84	63.8	139.2	150.8	174	40.6
	3.5	3.6	3.8	3.9	3.9	3.7
O	29.0	45.2	95.2	109.0	116.0	
	3.1	3.2	3.5	3.6	3.7	

the size of clusters by reducing the content of N_2 relative to that of helium in the gas jet led to an increase in the efficiency of N atom stabilization. As one can see in Table 1, the small increase in the stabilization efficiency by the addition of different quantities of neon atoms to the N_2–He gas mixtures might also be explained due to differences in the size of the nanoclusters. However, the results of the measurements of the average concentrations of N atoms in N_2–Ar–He and N_2–Kr–He condensates show that argon and especially krypton atoms play a very important role in increasing the overall efficiency of the stabilization of N atoms. As we can see in Fig. 4, N_2/Ne and N_2/Ar ratios in gas mixtures are the same, but the average concentration of N atoms stabilized in N_2–Ar–He samples is considerably higher than that obtained for samples containing neon atoms. In addition, when Ar atoms are added to N_2/He mixtures, the number of N atoms injected into the sample cell is about five times lower than when Ne atoms are added to the N_2/He mixtures (see Table 2). Previous studies of H–H_2–Kr–He and D–D_2–Kr–He condensates have also demonstrated that the addition of Kr atoms to the condensed H_2–He or D_2–He gas mixture leads to a substantial increase in the average concentration of stabilized hydrogen and deuterium atoms in the sample [11,12,33].

In Table 4, the parameters of interaction potentials of atoms and molecules forming impurity-helium condensates are presented. As can be seen from Table 4, van der Waals interactions between Ar–Ar and Kr–Kr are much stronger than for Ne–Ne atoms [32], so for the case of injection of N_2–Ar–He and N_2–Kr–He jets into superfluid helium, the Ar and Kr atoms initially form cores of the clusters. After that, N atoms and N_2 molecules are attached to the surface of the Ar or Kr cores of nanoclusters. In a previous study, it was shown that the nanoclusters in a sample prepared from the mixture N_2–Kr–He and N_2–Xe–He exhibit a shell structure [17,23]. We expect that the nanoclusters in

the sample prepared from the mixture N_2–Ar–He should also exhibit a shell structure due to the stronger van der Waals interaction between Ar–Ar atoms compared with that for the N_2–Ar interaction. From the analysis of the ESR spectra shapes (see Table 2), we can conclude that most of the N atoms (70–80%) reside on the surfaces of N_2 layers, another fraction of the N atoms resides inside the N_2 layer (1–10%), and 13–20% of N atoms reside inside the Ar core of the clusters. On the other hand, the shell structure of the nanoclusters prepared from gas mixtures containing (N–N_2–Ne–He) is quite different. After the jet cools down, first the nanoclusters of N_2 are formed, and later N atoms bind to the surface of the N_2 nanoclusters. At the next stage, the layers of Ne atoms surround the nanoclusters, and finally, a few layers of solidified helium atoms cover the nanoclusters. To prove this model, we also performed an analysis of the ESR spectra of N atoms after annealing to 10 K. For the nitrogen–argon–helium sample upon annealing in Fig. 8c, the nitrogen atoms residing in N_2 layers diffuse rapidly, destroying a majority of the surface population of the nitrogen atoms by fast recombination and leaving only a small population of nitrogen atoms surviving in Ar nanocluster cores. In the case of nitrogen–neon–helium samples (see Fig. 8a), during annealing, the nitrogen atoms almost completely recombined in the outer layer of neon atoms covering cluster cores formed by N_2 molecules. Only nitrogen atoms residing inside these N_2 cluster cores partially survived after the annealing process. The data from analysis of Fig. 8 are represented in the lowest three entries of Table 3. Other entries in Table 3 correspond to the g and A values for N atoms in different rare gas matrices which were obtained by other authors. Our results gave reasonable quantitative agreement with the experimental values of g and A obtained in previous work for N atoms in N_2 and rare gas matrices.

To determine the influence of warming on the concentration of nitrogen atoms, we investigated samples condensed from nitrogen–argon–helium and nitrogen–neon–helium mixtures. After performing ESR measurements on as-prepared samples at $T = 1.33$ K, the samples were heated to 2.16 K by ceasing pumping on the helium vapor from the sample. It is worth noting that the samples remain inside the superfluid helium during the entire period of warming. The observation of thermoluminescence of the samples in HeII during warming from 1.33 to 2.16 K and the stability of the ESR signal during the heating process in HeII have been explained in our previous publication [30]. The challenge of this work is to keep the impurity-helium condensates stable while above the lambda temperature to prevent rapid recombination of free radical impurities and structural changes in all samples. Usually in the annealing process, a majority of N atoms can survive in the samples up to the temperature 5 K. This perhaps might be important for energy storage purposes and possible rocket fuel applications. An increase in the N atom ESR signals at $T \sim 5$ K (see Fig. 6) can be explained by the collapse of the pores in the sample, which causes an increase in the sample density and the possibility that an additional part of the sample can enter into the sensitive region of the ESR cavity. The average concentrations of the stabilized nitrogen atoms in the annealed samples increased by a factor of 2 and 4, respectively, for N–N_2–Ne–He and N–N_2–Ar–He samples (see Fig. 6). When the liquid helium was removed from the pores, the resulting dry solid still retained its integrity. Once the liquid helium has evaporated, a rapid recombination process begins above 5 K with a series of bright flashes indicating that explosive chemical reactions have taken

Table 5 Comparison of highest average and local concentrations of nitrogen atoms stabilized in IHCs and their thermal stability (T_{st})

Gas mixture	n_{av}^{max}, $*10^{-18}$ cm^{-3}	ΔH_{pp}, G	n_{loc}^{rmmax}, $*10^{-20}$ cm^{-3}	Weight, %	T_{st}, K
$[N_2]$:[Ne]:[He] = 1:1:50	9				
$[N_2]$:[Ne]:[He] = 1:1:50		28.5	3.4	70–75	≤ 5
$[N_2]$:[Ar]:[He] = 1:1:200	10				
$[N_2]$:[Ar]:[He] = 1:5:600		27.4	3.3	70–80	≤ 5
$[N_2]$:[Kr]:[He] = 1:2:600	54 (Ref. [23])				
$[N_2]$:[Kr]:[He] = 1:2:600		77	9.3 (Ref. [23])	80–90	≤ 3
$[N_2]$:[Xe]:[He] = 10:1:2000	3.5 (Ref. [17])[a]				
$[N_2]$:[Xe]:[He] = 1:1:400		45	5.4 (Ref. [17])	75–80	[a]
$[N_2]$:[He] = 1:100	10 (Ref. [34])				
$[N_2]$:[He] = 1:400		45.8	8 (Ref. [34])	70	≤ 4

[a]Nitrogen–xenon–helium condensates were unstable even in bulk HeII

place. The broad feature of the ESR signal disappeared, and there only remained a small signal corresponding to the N atoms stabilized inside the Ar matrix (see Fig. 7).

Table 5 shows comparisons of average and local concentrations of N atoms in different impurity-helium condensates. The largest average, $N_{av} \sim (2-4) \times 10^{19}$ cm^{-3}, and local, $N_{loc} \sim (1.7-2.1) \times 10^{21}$ cm^{-3}, concentrations of N atoms were obtained for nitrogen–krypton–helium solids. For nitrogen–helium, nitrogen–argon–helium, and nitrogen–xenon–helium condensates, the highest local and average concentrations of stabilized N atoms were achieved by using different gas mixtures. The much larger local concentration of N atoms is an expected consequence of the high porosity of the impurity-helium samples. Impurity-helium condensates containing Xe atoms form structures with high energy content, which are unstable even inside superfluid ^{4}He. Also in Table 5, the relative weight of the atoms residing on the surfaces of the nanoclusters (70–90%) is shown. These weights were obtained from analysis of the ESR spectra of N atoms. It is surprising that most of the N atoms reside on the surface of N_2 layers covering cores of nanoclusters composed of heavy rare gas atoms (Ar, Kr, Xe).

5 Conclusion

1. Argon and especially krypton atoms play a crucial role in increasing the overall efficiency for the stabilization of N atoms in impurity-helium condensates. Conversely, the addition of neon atoms to nitrogen–helium gas mixtures does not affect the stabilization efficiency of the N atoms.
2. Decreasing the size of the clusters by reducing the nitrogen content of the gas jet resulted in an increase in the efficiency of stabilization of N atoms partially due to higher specific surface area of smaller clusters.

3. The ESR spectra of N atoms in the nitrogen–argon–helium and nitrogen–krypton–helium samples were different from the nitrogen–neon–helium samples indicating different distributions of N atoms in nanoclusters. The ESR spectra in the annealed nitrogen–argon–helium and nitrogen–krypton–helium samples revealed Ar and Kr cores of nanoclusters while ESR of N atoms in the annealed nitrogen–neon–helium samples indicated nitrogen cores of nanoclusters.
4. Warming IHC samples to 5 K increases the average concentration of nitrogen atoms up to four times.
5. Stabilization by matrix isolation of highly reactive atoms in IHCs leads to high concentrations of these atoms even in samples removed from liquid helium. Our results reveal that up to 70–90% of stabilized nitrogen atoms residing on the impurity nanoclusters surfaces do not recombine due to the presence of shells of solidified helium.

Acknowledgements This work was supported by NSF Grant No. DMR 1707565.

References

1. L. Vegard, Nature **113**, 716 (1924a)
2. L. Vegard, Nature **114**, 357 (1924b)
3. A.M. Bass, H.P. Broida, Phys. Rev. **101**, 1740 (1956)
4. A.M. Bass, H.P. Broida, *Formation and Trapping of Free Radicals* (Academic Press, New York, 1960)
5. E.B. Gordon, L.P. Mezhov-Deglin, O.F. Pugachev, JETP Lett. **19**, 63 (1974)
6. E.B. Gordon, L.P. Mezhov-Deglin, O.F. Pugachev, V.V. Khmelenko, Cryogenics **16**, 555 (1976)
7. E.B. Gordon, V.V. Khmelenko, E.A. Popov, A.A. Pelmenev, O.F. Pugachev, Chem. Phys. Lett. **155**, 301 (1989)
8. V. Kiryukhin, B. Keimer, R.E. Boltnev, V.V. Khmelenko, E.B. Gordon, Phys. Rev. Lett. **79**, 1774 (1997)
9. S. Kiselev, V.V. Khmelenko, D.M. Lee, V. Kiryukhin, R.E. Boltnev, E.B. Gordon, B. Keimer, Phys. Rev. B **65**, 024517 (2002)
10. E.P. Bernard, V.V. Khmelenko, D.M. Lee, J. Low Temp. Phys. **150**, 516 (2008)
11. R.E. Boltnev, E.P. Bernard, J. Jarvinen, V.V. Khmelenko, D.M. Lee, Phys. Rev. B **79**, 180506 (2009)
12. R.E. Boltnev, E.P. Bernard, J. Jarvinen, I.N. Krushinskaya, V.V. Khmelenko, D.M. Lee, J. Low Temp. Phys. **158**, 468 (2010)
13. E.P. Bernard, R.E. Boltnev, V.V. Khmelenko, V. Kiryukhin, S.I. Kiselev, D.M. Lee, Phys. Rev. B **69**, 104201 (2004)
14. R.E. Boltnev, I.N. Krushinskaya, A.A. Pelmenev, D.Y. Stolyarov, V.V. Khmelenko, Chem. Phys. Lett. **305**, 217 (1999)
15. V.V. Khmelenko, D.M. Lee, I.N. Krushinskaya, R.E. Boltnev, I.B. Bykhalo, A.A. Pelmenev, Low Temp. Phys. **38**, 688 (2012)
16. V.V. Khmelenko, A.A. Pelmenev, I.N. Krushinskaya, I.B. Bykhalo, R.E. Boltnev, D.M. Lee, J. Low Temp. Phys. **171**, 302 (2013)
17. R.E. Boltnev, I.B. Bykhalo, I.N. Krushinskaya, A.A. Pelmenev, V.V. Khmelenko, S. Mao, A. Meraki, S.C. Wilde, P.T. McColgan, D.M. Lee, J. Phys. Chem. A **119**, 2438 (2015)
18. A. Meraki, S. Mao, P.T. McColgan, R.E. Boltnev, D.M. Lee, V.V. Khmelenko, J. Low Temp. Phys. **158**, 468 (2016)
19. S.I. Kiselev, V.V. Khmelenko, E.P. Bernard, D.M. Lee, Low Temp. Phys. **29**, 505 (2003)
20. S.I. Kiselev, V.V. Khmelenko, E.P. Bernard, C.Y. Lee, D.M. Lee, Physica B **329–333**, 377 (2003)
21. E.P. Bernard, R.E. Boltnev, V.V. Khmelenko, D.M. Lee, J. Low Temp. Phys. **138**, 829 (2005)
22. S. Mao, A. Meraki, P.T. McColgan, V. Shemelin, V.V. Khmelenko, D.M. Lee, Rev. Sci. Instrum. **85**, 073906 (2014)
23. S. Mao, R.E. Boltnev, V.V. Khmelenko, D.M. Lee, Low Temp. Phys. **38**, 1037 (2012)
24. R. Beringer, M.A. Heald, Phys. Rev. **95**, 1474 (1954)

25. Yu.A. Dmitriev, R.A. Zhitnikov, Low Temp. Phys **24**, 44 (1998)
26. P.H.H. Fischer, S.W. Charles, C.A. McDowell, J. Chem. Phys. **46**, 2162 (1967)
27. J. Eloranta, K. Vaskonen, H. Hakkanen, T. Kiljunen, H. Kunttu, J. Chem. Phys. **109**, 7784 (1998)
28. L.B. Knight, J. Steadman, J. Chem. Phys. **77**(4), 1750 (1982)
29. C. Kittel, E. Abrahams, Phys. Rev. **90**, 238 (1953)
30. A. Meraki, P.T. McColgan, P.M. Rentzepis, R.Z. Li, D.M. Lee, V.V. Khmelenko, Phys. Rev. B **95**, 104502 (2017)
31. E.B. Gordon, Low Temp. Phys. **30**, 756 (2004)
32. A.A. Radtsig, B.M. Smirnov, *Reference Book on Atomic and Molecular P* (Atomizdat, Moscow, 1980)
33. R.E. Boltnev, V.V. Khmelenko, D.M. Lee, Low Temp. Phys. **36**, 382 (2010)
34. E.P. Bernard, R.E. Boltnev, V.V. Khmelenko, D.M. Lee, J. Low Temp. Phys. **134**, 199 (2004)